Med Biol Eng Comput (2011) 49:985–995
DOI 10.1007/s11517-011-0791-6

ORIGINAL ARTICLE

An EEG-based real-time cortical functional connectivity imaging system

Han-Jeong Hwang · Kyung-Hwan Kim · Young-Jin Jung · Do-Won Kim · Yong-Ho Lee · Chang-Hwan Im

Received: 11 October 2010 / Accepted: 13 June 2011 / Published online: 24 June 2011

Abstract In the present study, we introduce an EEG-based, real-time, cortical functional connectivity imaging system capable of monitoring and tracing dynamic changes in cortical functional connectivity between different regions of interest (ROIs) on the brain cortical surface. The proposed system is based on an EEG-based dynamic neuroimaging system, which is capable of monitoring spatio-temporal changes of cortical rhythmic activity at a specific frequency band by conducting real-time cortical source imaging. To verify the implemented system, we performed three test experiments in which we monitored temporal changes in cortical functional connectivity patterns in various frequency bands during structural face processing, finger movements, and working memory task. We also traced the changes in the number of connections between all possible pairs of ROIs whose correlations exceeded a predetermined threshold. The quantitative analysis results were consistent with those of previous off-line studies, thereby demonstrating the possibility of imaging cortical functional connectivity in real-time. We expect our system to be applicable to various potential applications, including real-time diagnosis of psychiatric diseases and EEG neurofeedback.

Keywords Electroencephalography (EEG) · Functional connectivity · Real-time neuroimaging · Diagnosis of psychiatric diseases · Inverse problems

1 Introduction

Traditional functional neuroimaging studies have focused on either functional mapping of brain areas or investigation of task-dependent changes in brain activities; however, such studies can only provide a limited amount of information with respect to underlying neuronal processes. Recently, an increasing number of neuroscientists have become interested in describing the communications between different brain areas, since such information might be helpful for better understanding the functional networks of cortical regions [7, 13, 15, 23, 29, 40, 45]. Generally, functional interactions among different cortical areas, typically referred to as functional connectivity, can be measured using linear or nonlinear analysis of time series extracted from various brain imaging techniques such as functional magnetic resonance imaging (fMRI) [15], near infrared spectroscopy (NIRS) [23], electroencephalography (EEG), and magnetoencephalography (MEG) [7, 13, 29, 40, 45].

EEG and MEG are believed to be more suited for studying interactions among brain areas at the level of cognitive processes due to their superior temporal resolutions as compared to hemodynamics-based imaging

H-.J. Hwang and K.-H. Kim are co-first authors and contributed equally to this work.

Electronic supplementary material The online version of this article (doi:10.1007/s11517-011-0791-6) contains supplementary material, which is available to authorized users.

H.-J. Hwang · Y.-J. Jung · D.-W. Kim · C.-H. Im (✉)
Department of Biomedical Engineering, Hanyang University, 17 Haengdang-dong, Seongdong-gu, Seoul 133-791, South Korea
e-mail: ich@hanyang.ac.kr

H.-J. Hwang · K.-H. Kim · Y.-J. Jung · D.-W. Kim
Department of Biomedical Engineering, Yonsei University, Wonju, Korea

Y.-H. Lee
Korea Research Institute of Standard and Science, Daejeon, Korea

modalities such as fMRI and NIRS [7, 30]. Indeed, functional connectivity analyses based on scalp EEG and MEG have been applied extensively to a variety of practical applications including functional characterization of neuropsychiatric diseases [32, 41, 44], noninvasive diagnosis of psychiatric diseases by quantifying global synchronization [28, 43, 46], and investigation of functional networks associated with various cognitive processes [10, 27]. Further, freely available MATLAB toolboxes for the functional connectivity analysis are widely available [8, 47].

At present, despite recent advances in technology, estimation of functional connectivity from sensor level recordings has been met with severe criticism from many neuroscientists, as these recordings can be corrupted by the effect of volume conduction (or field spread). Indeed, simulation studies have shown that field spread can lead to misinterpretation of connectivity estimates between some pairs of sensors [49] because scalp potentials recorded from scalp EEG are not usually directly attributed to the underlying cortical regions. However, recent developments in source imaging techniques have made possible the ability to estimate temporal changes in underlying cortical sources; functional connectivity can now be estimated at the cortical source level [1, 18]. Therefore, the functional connectivity estimation at the cortical source level has been gradually replacing sensor-level analyses.

To the best of our knowledge, however, real-time imaging of cortical functional connectivity at the cortical source level has not been introduced, despite the rapid developments in computational neuroimaging. Implementation of such a real-time imaging of cortical functional connectivity may be a promising tool for practical applications. For example, such a system could be used as an auxiliary diagnosis tool to provide a prompt measure reflecting a subject's brain responses to certain stimuli, thereby helping patients with neuropsychiatric diseases such as dementia and schizophrenia as well as their relatives to accept diagnostic results [54], since people are apt to put more confidence in high-tech medical diagnostic devices than they are in traditional paper-based diagnosis methods such as the mini-mental state examination (MMSE) and positive and negative symptom scale (PANSS). Moreover, the real-time cortical functional connectivity imaging system can be used for EEG neurofeedback applications, as many researchers have been interested in monitoring dynamics of functional connectivity during neurofeedback treatment [4–6, 21]. Potential applications of real-time imaging of cortical functional connectivity will be discussed more in Sect. 4.

The aim of the present study was to realize a real-time cortical functional connectivity imaging system capable of monitoring and tracing temporal changes in source-level connectivity between different regions of interest (ROIs) on the cortical surface. To implement this system, scalp EEG signals were converted into frequency domain datasets in real-time and mapped onto cortical source space by applying frequency domain inverse estimation. Then, the cortical signals were spatially grouped for each ROI and analyzed in order to find the correlations among the ROIs. To demonstrate the feasibility of the implemented system, we performed three test experiments in which we monitored the changes in cortical functional connectivity patterns while the participants were performing different tasks.

2 Methods

2.1 Methods for real-time connectivity imaging

The proposed cortical functional connectivity imaging system is based on the EEG-based real-time cortical rhythmic activity monitoring system [22], hereafter referred to as a real-time dynamic neuroimaging system. The real-time dynamic neuroimaging system could visualize spatiotemporal changes in cortical rhythmic activity of a specific frequency band on a subject's cortical surface, rather than the subject's scalp surface, with a high temporal resolution. Recently, the real-time imaging system was successfully applied to a neurofeedback-based motor imagery training system that can help individuals to more easily become accustomed to motor imagery tasks [20]. In this section, we will first introduce the brief concepts of the real-time dynamic neuroimaging system and then describe the technical details of the real-time cortical functional connectivity imaging system.

The EEG-based real-time dynamic neuroimaging system [22] consisted of pre-processing and real-time processing parts. In the pre-processing part, a linear inverse operator was constructed in which the subject's anatomical information was reflected. Once the linear inverse operator had been constructed and saved to a data-storage unit, spatiotemporal changes in cortical rhythmic activities could be monitored in real-time by means of a unified processing scheme consisting of three independent programs, namely, a fast Fourier transform (FFT) program, a frequency domain minimum norm estimation (FD-MNE) solver, and a 3D visualization program, which were executed sequentially at each time slice.

The proposed cortical functional connectivity imaging system shares the same platform with the real-time dynamic neuroimaging system except for the 3D visualization program. Instead of calculating the absolute current source power at cortical vertices with respect to the frequency band of interest, the proposed system calculates instantaneous source power changes for each frequency of interest. The detailed processes are described below.

To reconstruct the cortically distributed brain sources, we used a linear estimation approach. The expression for the inverse operator **W** was defined as

$$\mathrm{W} = \mathrm{RA}^{\mathrm{T}}\left(\mathrm{ARA}^{\mathrm{T}} + \lambda^2\mathrm{C}\right)^{-1}, \quad (1)$$

where **A** is a lead field matrix, which represents impulse response of each source vector component at every measurement site, **R** is a source covariance matrix representing inter-source relationship, which is hardly estimated without using intracranial recordings, and **C** is a noise covariance matrix [33]. If we assume that both **R** and **C** are scalar multiples of identity matrix, this approach becomes identical to minimum norm estimation [34]. In this study, the source covariance matrix **R** was assumed to be an identity matrix, which means that we ignored relationships between neighboring sources. In this study, background environmental noise acquired before attaching electrodes on the subject's scalp was used to calculate **C** [33]. λ^2 is a regularization parameter and was determined systematically based on the signal-to-noise ratio [33]. Once a specific frequency band was determined, the FFT program calculated real and imaginary components at all discrete frequencies within the predetermined frequency band. Instead of using wavelet transform [33], we used FFT to obtain constant time–frequency resolution. Then, the FD-MNE solver was executed, which loads the Fourier transformed signals $\mathbf{B}(f_i)_{\mathrm{Re}}$ and $\mathbf{B}(f_i)_{\mathrm{Im}}$, $i = 1, 2, \ldots, n$, where Re and Im represent the real and imaginary parts of the Fourier transformed signals, respectively, as well as the pre-saved inverse operator **W**. The real part $\mathbf{q}_j(f_i)_{\mathrm{Re}}$ and imaginary part $\mathbf{q}_j(f_i)_{\mathrm{Im}}$ of the current source vector at the jth cortical vertex with respect to the frequency of interest f_i can then be evaluated by multiplying the corresponding rows ($3j - 2$, $3j - 1$, and $3j$th rows) in **W** with the Fourier transformed signals $\mathbf{B}(f_i)_{\mathrm{Re}}$ and $\mathbf{B}(f_i)_{\mathrm{Im}}$. We used the FD-MNE method instead of time-domain MNE method to estimate the current source vectors because under the current computing environment maximally 20–30 source images could be calculated per every second due to the computational time required for the inverse process [22]. Then, the instantaneous source power changes for a frequency f_i at the jth cortical vertex can be readily estimated by inverse Fourier transforming each directional component (x, y, z-directional components) of $\mathbf{q}_j(f_i)_{\mathrm{Re}}$ and $\mathbf{q}_j(f_i)_{\mathrm{Im}}$ into time-domain series ($q_{x,j}(t)$, $q_{y,j}(t)$, $q_{z,j}(t)$) and calculating the power of the source vector $Q_j(t_k)$ as $Q_j(t_k) = q_{x,j}(t_k)^2 + q_{y,j}(t_k)^2 + q_{z,j}(t_k)^2$ at densely discretized time samples (the subscript k represents kth time sample). After evaluating the instantaneous source powers at every cortical vertex, the source powers are averaged over all cortical vertices included in each ROI (see Fig. 1b in advance), yielding the instantaneous source power changes of each ROI, $RQ_l(t_k)$, where the subscript l represents the lth ROI. For an ith frequency of interest, f_i, the functional connectivity between the mth and nth ROIs was evaluated by simply calculating the correlation coefficient (CC) between the two signal power time series extracted from the two ROIs, $\mathrm{CC}_{m,n}(f_i)$. Finally, the CC values evaluated for all possible pairs of ROIs were averaged over the frequency band of interest. ROI pairs in which the connectivity exceeded a predetermined threshold CC value were visualized as a straight line connecting the two ROIs (see Fig. 2 in advance).

2.2 EEG recording environments

Scalp EEG readings were recorded at 32 electrode locations (Cz, C3, T7, C4, T8, Fz, F3, F7, F4, F8, AFz, AF7, AF8, FP1, FP2, FC5, FC1, FC2, FC6, Pz, P7, P3, P4, P8, CP5, CP1, CP2, CP6, O1, O2, PO3, and PO4) using a 32-channel EEG acquisition system (WEEG-32, Laxtha Inc., Daejoen, Korea) in a dimly lit, soundproof room. The electrodes were attached to the subject's scalp according to the extended 10–20 system without using an electrode cap. The ground electrode was placed behind the left ear with the reference electrode on the opposite side. The EEG signal was sampled at 512 Hz, and the low- and high-pass filters were set at 64 and 0.5 Hz cutoffs (12 dB/octave), respectively, in all experiments. To implement the 'real-time' imaging system, we did not apply any time-consuming signal preprocessing methods for noise/artifact removal to the input EEG signals.

2.3 Implementation of a real-time cortical connectivity imaging system

In the present study, a standard brain atlas [9] provided by the Montreal Neurological Institute (MNI) and a standard configuration of EEG electrodes were utilized, since individual magnetic resonance imaging (MRI) data for the subjects were not available. A first-order node-based boundary element method (BEM) was applied to construct a leadfield matrix. In the present study, three-layer tessellated boundary surfaces, consisting of inner and outer skull boundaries and scalp surface, were generated using CURRY6 for windows (Compumedics, Inc., El Paso, TX) from the standard structural MRI data. The conductivity values of brain, skull, and scalp were assumed to be 0.22, 0.014, and 1.79 S/m, respectively [16, 42]. Coordinate transformation and electrode positioning were performed using in-house software, 'BioEST' (http://bem.yonsei.ac.kr). For the extraction and tessellation of the cortical surface models, we applied *BrainSuite* developed in the University

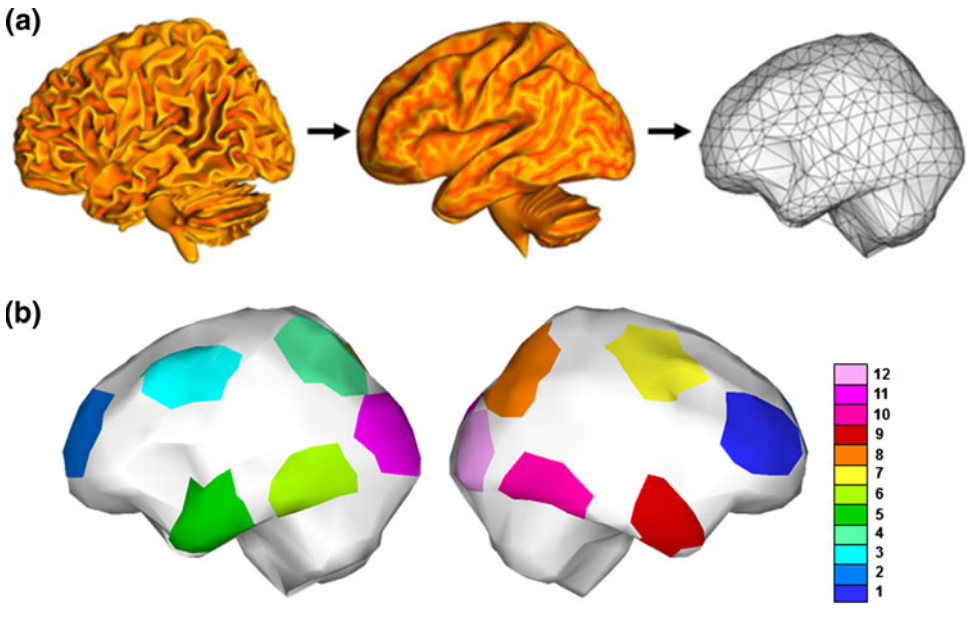

Fig. 1 **a** Process of generating cortical source space: a high-resolution cortical surface was smoothed and down-sampled for the real-time source imaging. **b** Locations of 12 regions of interest (ROIs): *colors* represent the ROI number (see the *color bar* on the *right side*). (Color figure online)

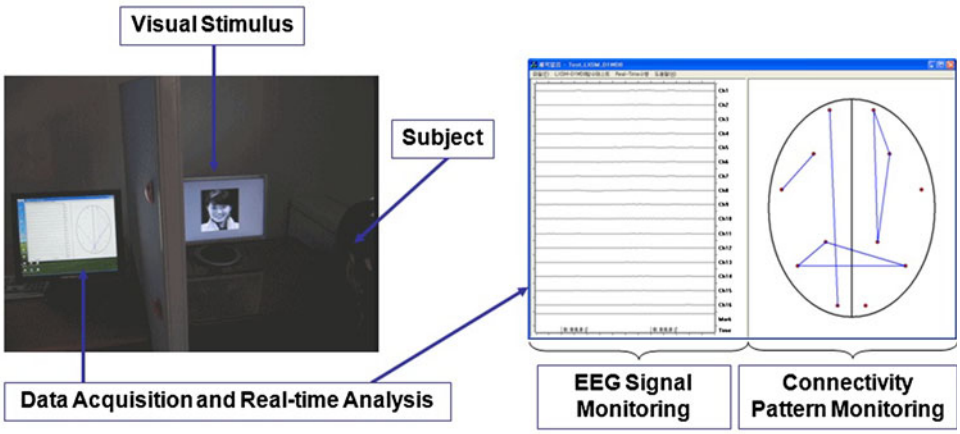

Fig. 2 A snapshot of a test experiment (*left*), and a screenshot of the real-time cortical functional connectivity monitoring software (*right*): dual LCD monitors were connected to a single computer system and were separated with a partition. The monitoring software can visualize both the on-going EEG signals and the current connectivity patterns

of Southern California, CA, USA [50]. To reduce the number of possible cortical source locations, we first smoothed the cortical surface [11] and generated a down-sampled epi-cortical surface with approximately 1,000 cortical vertices. Figure 1a shows the processes for generating the cortical source space, on which the equivalent dipole sources were placed, from standard brain MRI data. Since we used the smoothed cortical surface model as the source space, source orientation constraints were not imposed. Figure 1b shows the 12 ROIs, of which the locations and sizes were determined according to the following two criteria: (1) whole brain regions have to be taken into account in order to be applicable to a variety of experimental paradigms; and (2) the number of ROIs should not be too many for the real-time processing. Considering the above conditions, we selected six ROIs on each hemisphere: two ROIs in the frontal lobe, two ROIs in the temporal lobe, one ROI in the parietal lobe, and one ROI in the occipital lobe. The main reason why we used approximated and downsampled cortical surface as well as assumed relatively small number of ROIs was that using realistic cortical surface model and many ROIs would increase the computational cost, thereby making the 'real-time' processing difficult. Since the computer system is being developed very rapidly, we believe that more realistic real-time connectivity imaging system would be available in the near future.

Figure 2 shows a snapshot of our test experiments. Dual LCD monitors were connected to a high-performance personal computer system (Intel Core2-6300 1.86 GHz environment) and were separated with a partition not to disturb the participants' attention. Visual stimuli were presented through an LCD monitor placed in front of the participant. Cortical functional connectivity patterns as well as the on-going EEG signals were visualized on the other LCD monitor. During the real-time imaging, EEG

signals were transferred to the operating computer in real-time, and the values were stored in a two-dimensional array variable. At a specific time slice, time domain signals in 256 data samples before the time slice were transformed into frequency domain signals using FFT. After execution of the FD-MNE solver and connectivity calculation module, ROI pairs whose connectivity exceeded a predetermined threshold value were visualized as a straight blue line connecting the two ROIs that were depicted as small red dots in the connectivity pattern monitoring software (see Fig. 2). The real-time cortical connectivity monitoring software was designed to store every instantaneous connectivity pattern as well as the stimulus onset times into the storage unit. We updated the cortical connectivity maps at 250 ms intervals (four image frames/second).

3 Results

To verify the feasibility of the implemented system, we monitored the temporal changes in cortical functional connectivity patterns while participants were performing different tasks. We performed three test experiments: (Exp. 1) monitoring gamma band cortical connectivity changes associated with structural face processing; (Exp. 2) monitoring alpha and beta band connectivity changes during finger movement; and (Exp. 3) monitoring theta band connectivity changes during working memory task.

Six healthy volunteers (six males, all right handed, mean age 25.5 years; range 21–29 years) took part in the first experiment (Exp. 1) and three healthy volunteers (three males, all right handed, mean age 26 years, range 24–28 years) participated in the second and third experiments (Exp. 2 and Exp. 3). None of the participants had a previous history of neurological, psychiatric, or other severe diseases that may otherwise have influenced the experimental results. We gave a fully detailed summary of the experimental procedures and protocols to each of the participants before the experiment. The study protocol was approved by the Institutional Review Board of Yonsei University, Korea.

3.1 Gamma-band cortical connectivity monitoring (Exp. 1)

In our first test experiment, we attempted to track temporal changes in cortical functional connectivity patterns during structural face recognition. One hundred full facial images of most famous Koreans (50 males and 50 females) were randomly presented to the participants through a 17″ LCD monitor. Original color pictures were converted to gray-scale images with identical sizes and resolutions. The facial images were randomly shuffled and were presented to the participants for 1 s. Every image appeared only once throughout the whole experiment. The reason why we converted the color images into gray-scale images was that the face images used for the present study had various background colors and different chroma characteristics, which might influence some ERP components such as P1, N1, and selection negativity, according to the previous relevant studies [12, 17, 19]. Therefore, many EEG experiments associated with face recognition have used gray-scale face images [2, 31, 55].

The inter-stimulus interval (ISI) was set as 5 s, during which only a gray (RGB: 132, 132, 132) background was presented (see the Supplementary movie file). Recordings were conducted in a single session consisting of 50 trials. Thus, the entire experiment lasted for approximately 5 min. During the recordings, the participants were sat in a comfortable armchair. In order to keep the participants attention, they were asked to count the number of unfamiliar faces, but were not required to provide any physical response. After the experiment, we found that the number of unfamiliar faces was less than five for all of the participants. According to a previous literature [31] that used similar experimental paradigm, the cortical connectivity changes were mainly associated with face structural processing. We also confirmed from some preliminary experiments that counting the number of unfamiliar faces did not influence the main experimental outcomes. We set the frequency band of interest as 30–40 Hz to observe the time-varying gamma-band synchronization. We did not apply any signal processing algorithms [26, 38] for removing artifacts potentially originated from micro-saccades since those algorithms generally required significant computational cost and thus did not seem to be adequate for the real-time signal processing.

Figure 3a shows some screenshots taken before and after the visual stimulus onset for one participant (subject JK), captured during the online experiment (see the Supplementary movie file). Figure 3b shows an example of the variation in the number of connections counted at each time slice (every 250 ms), where red arrows represent the visual stimulus onsets. It can be seen from the figures and the Supplementary movie file that the number of connections suddenly increased after the visual stimulus onset. The average numbers of connectivity connections observed during a 2-s period before and after presenting the facial images were counted and the ratios between the two values are presented in Table 1. It can be seen from the table that the number of connectivity connections after presenting the images were greater than that before presenting the images for any tested threshold CC values. We also applied a one-tail paired t test between the average numbers of connectivity connections counted before and after the stimulus onset, and found statistically significant increment

($P < 0.05$) in the number of connections for all cases considered in Table 1. In our experiments, we applied four different threshold CC values to all six subjects and found that the slight changes in the threshold value did not affect the main trend of the results—increment in the number of connections after the stimulus onset. Indeed, as presented in the Table 1, the use of higher threshold values seemed to result in more distinct connectivity changes. However, when we used higher threshold values exceeding 0.99, we could hardly observe the dynamic changes in connectivity patterns visually since the real-time connectivity imaging system did not show any connections at many time slices as found in the previous offline analysis studies [31, 53]. Therefore, we set the threshold CC value to 0.96 when we executed the online monitoring system to generate the results in Fig. 3. Since one of the main aims of the present system was to visually monitor the dynamic changes in the connectivity patterns, we allowed the potential users of our system to adjust the threshold CC values freely. According to our experience, in the online monitoring, the threshold CC value could be readily adjusted without performing any offline analyses by gradually changing the threshold value and continuously monitoring the changes in the connectivity patterns during a subject's resting state.

The results of our first test experiments are similar to the reports in [31] and [53], which showed the peaked gamma band activity synchronization around 200–400 ms after face images were presented. Moreover, according to the previous studies, the gamma band synchronization between different brain areas during the processing of facial structure is significantly reduced in schizophrenia patients [31, 53]. Based on the previous studies, we are planning to apply the present system to real-time diagnoses of schizophrenia, after conducting clinical examinations.

3.2 Alpha/beta-band cortical connectivity monitoring (Exp. 2)

In our second test experiment, we tracked the temporal changes in cortical functional connectivity patterns during finger movements. Since it has been widely known that finger movements can elicit connectivity increase in alpha/beta frequency bands [35], we set the frequency band of interest as 8–30 Hz. The three participants were sat in a comfortable armchair and were asked to touch the tip of the left thumb with the tip of the left index finger. Right after a pure tone beep sound was generated from the computer speaker, they were instructed to detach the two fingers for approximately 0.5 s and then touch the fingers again (see 4th figure of Fig. 4). The ISI was set as 5 s, during which only a cross fixation (+) was presented at the center of the computer monitor in front of the participants. The participants were also asked to stare the fixation mark during the entire experiments. Recordings were conducted in a single session consisting of 50 trials.

Figure 4 shows some screenshots taken before and after the stimulus onset (3rd figure of Fig. 4) for one participant (subject JI), captured during the online experiment. In the second and third experiments, we fixed the threshold CC value to 0.96, based on the experience attained from the first experiment. Then, the average numbers of connectivity connections observed during a 1.5-s period before and after the stimulus onset were also counted and the ratios between the two values were evaluated. The ratios for subjects JI, JJ, and JH were 2.14 ± 0.67, 2.87 ± 0.81, and 1.96 ± 0.39, respectively. It could be seen from the figure and the resultant ratio values that the number of connectivity connections was increased after finger movements, demonstrating that the alpha/beta band cortical connectivity changes elicited by finger movement could be monitored using the implemented system.

3.3 Theta-band cortical connectivity monitoring (Exp. 3)

In our third test experiment, we tracked the temporal changes in cortical functional connectivity patterns during working memory task. Our paradigm was devised based on the Sarnthein et al.'s [48] work, where the authors reported significant enhancement in theta band (4–7 Hz) connectivity between prefrontal and posterior areas. During 5-s perception period, the participants were presented with 6-digit randomly generated characters consisting of capital English letters and numbers (e.g., SD9FG4) through a 17″ LCD monitor located in front of each participant. During the next 5 s, the participants were instructed to memorize the given characters while staring the cross fixation (+) located at the center of the computer screen. Then, the participants were asked to verbally recall the characters that they memorized. The experimenter checked whether the answer was correct and then manually started the next trial. Before the new combinations of characters were presented, blank screen was presented to the participants for 5 s. Recordings were conducted in a single session consisting of 50 trials. The correct ratios evaluated for subjects JI, JJ, and JH were 88, 90, and 90%, respectively, which were similar to the results reported in the previous study [48].

Figure 5 shows some screenshots taken during the online experiment of one participant (subject JJ), captured at every 1.5 ms. As mentioned in the previous section, we fixed the threshold CC value to 0.96. It could be observed from Fig. 5 that the long-range connectivity between prefrontal area and posterior areas was notably increased during the 5-s retention period, coinciding well with the results of the previous offline study [48]. The average numbers of connectivity connections observed during the 5-s resting period and the

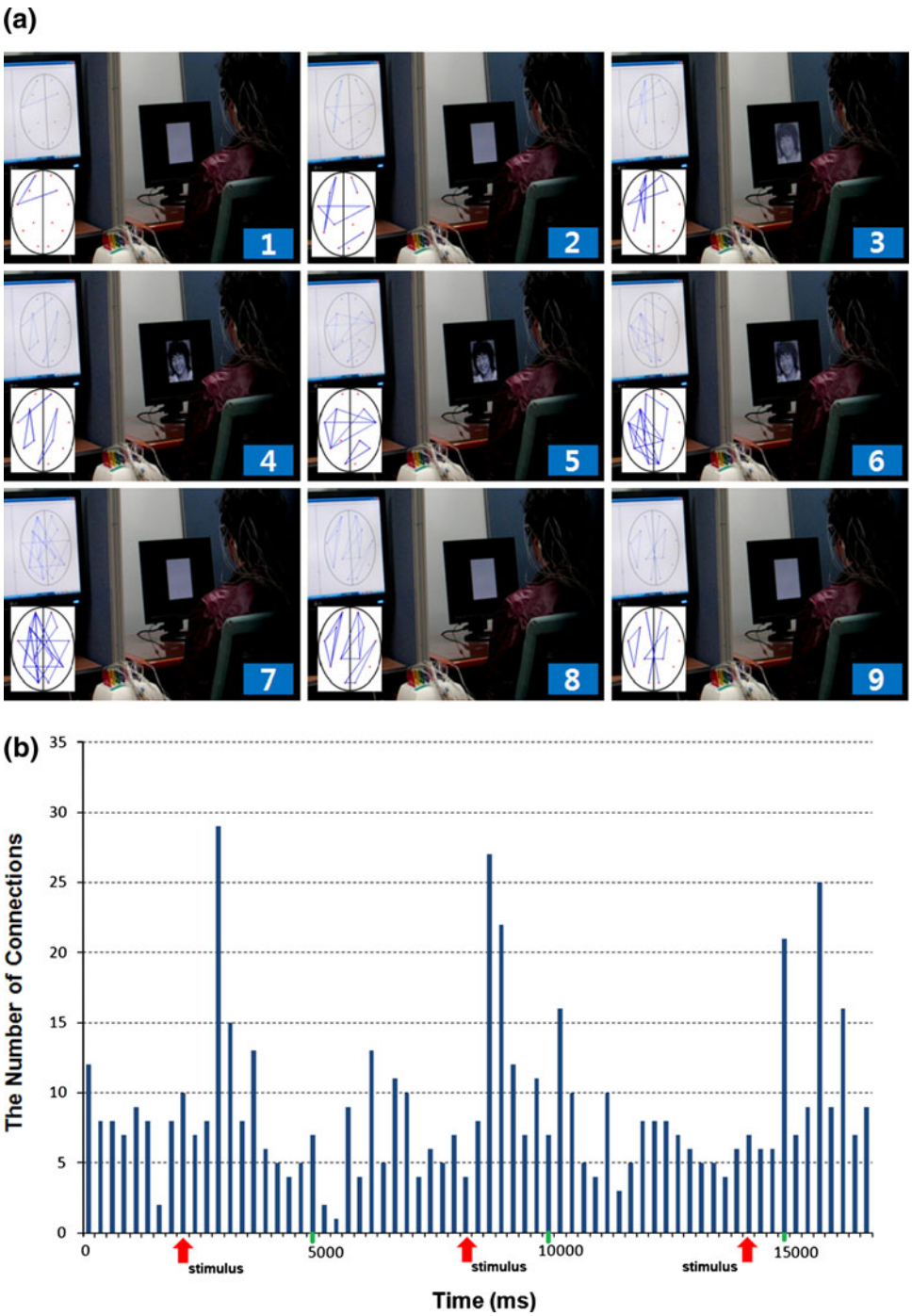

Fig. 3 Variations in the number of connections in the first experiment (Exp. 1) investigating the dynamics of gamma-band cortical connectivity: **a** Screenshots regularly sampled from the supplementary movie file (4 frames per second). *Numbers* in each picture represent the sequence of the pictures. Visual stimulus appeared in *third picture* and disappeared after *sixth picture*; **b** variation in the number of connections with respect to time: *arrows* represent stimulus onsets. The threshold was set to 0.96. These examples are parts of one participant's data (subject JK)

Table 1 The ratios of the average numbers of connectivity connections observed during a 2 s period after presenting the facial images to those observed during a 2 s period before presenting the images

Thresholds	YC	HJ	JK	MK	JL	IL
0.96	1.44 (0.49)	1.43 (0.77)	1.31 (0.61)	1.31 (0.36)	1.19 (0.35)	1.25 (0.46)
0.97	1.41 (0.49)	1.47 (0.87)	1.43 (0.97)	1.29 (0.38)	1.21 (0.37)	1.36 (0.68)
0.98	1.51 (0.63)	1.66 (0.91)	1.51 (1.12)	1.42 (0.43)	1.22 (0.47)	1.29 (0.87)
0.99	1.55 (0.65)	2.09 (1.72)	3.06 (2.86)	1.75 (1.33)	1.35 (0.77)	1.40 (1.19)

YC, HJ, JK, MK, JL, and IL represent initials of the participants. Values in parentheses are standard deviations

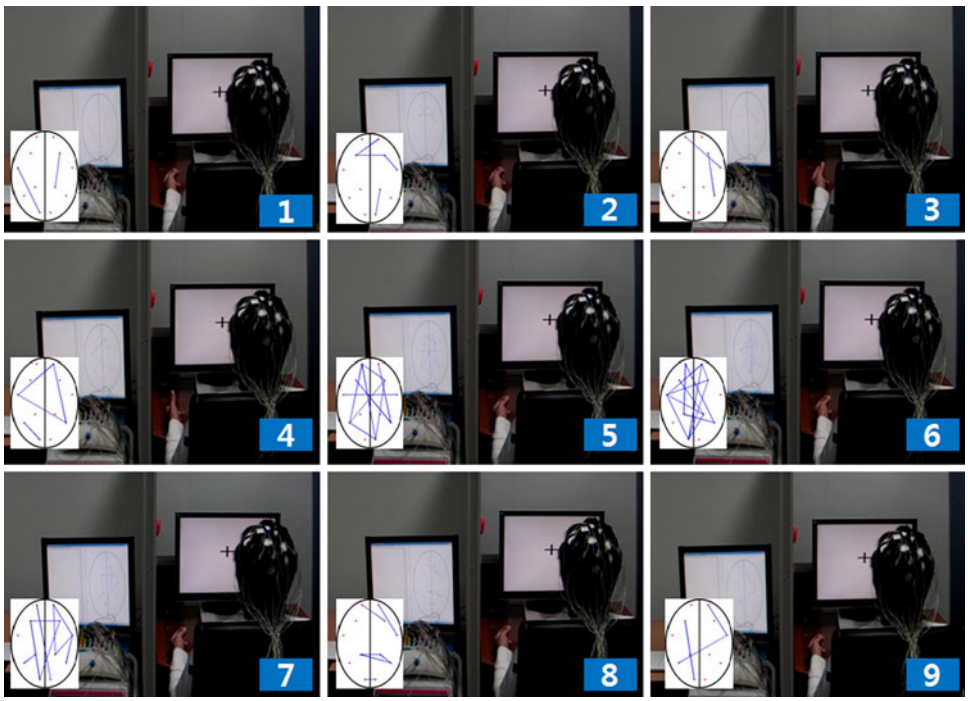

Fig. 4 Variations in the number of connections in the second experiment (Exp. 2) investigating the dynamics of alpha/beta-band cortical connectivity: Screenshots regularly sampled from a movie file (2 frames per second). *Numbers* in each picture represent the sequence of the pictures. The subject moved his *left fingers* in *fourth picture*

Fig. 5 Variations in the number of connections in the third experiment (Exp. 3) investigating the dynamics of theta-band cortical connectivity: Screenshots regularly sampled from a movie file (1.5-s interval). Numbers in each picture represent the sequence of the pictures. A 6-digit word was presented in *third picture* and the retention interval started in *sixth picture*

5-s retention period were counted and the ratios between the two values were evaluated. The ratios for subjects JI, JJ, and JH were 3.01 ± 1.13, 2.57 ± 0.65, and 3.43 ± 0.97, respectively, demonstrating that the theta band cortical connectivity changes associated with working memory could be monitored using the implemented system.

4 Discussion

In the present study, we introduced an EEG-based, real-time, cortical functional connectivity imaging system, which can monitor the dynamic changes in cortical functional connectivity between different ROIs on the cortical

surface. To testify the implemented pilot system, we performed three test experiments in which we could monitor the real-time changes in cortical connectivity patterns in gamma, alpha/beta, and theta frequency bands.

Since we adopted a source-level connectivity analysis, our real-time imaging system is not subject to the hypothesis that EEG synchrony computed from scalp EEGs may contain spurious synchronizations resulting from volume conduction [39, 49]. Although in the present study we simply traced the real-time changes in the overall connectivity patterns, our system can be readily modified for investigating the changes in the connectivity strength between specific cortical ROIs as well as for characterizing the specific spatial patterns in the connectivity maps, e.g., hemispheric lateralization of the connectivity pattern; in either case, the source-level connectivity analysis is more appropriate than the sensor-level connectivity analysis. In our third test experiment (Exp. 3), which monitored dynamic cortical connectivity changes during working memory task, increment of connectivity between prefrontal and posterior cortical areas was observed, demonstrating the possibility of using our system for investigating dynamic spatial patterns in functional connectivity. In addition, the resultant connectivity patterns obtained from the source-level connectivity analysis can be less dependent upon the changes in the electrode than those from the sensor-level analysis because the source-level analysis projects the sensor-level recordings to the cortical source-level signals by solving an inverse problem.

Nevertheless, some issues associated with the source-level connectivity analysis should be investigated further in future studies. In the present study, we selected a simple power-to-power correlation for the calculation of functional connectivity between two ROIs because it was not possible to extract source time series at cortical vertices when minimum norm estimation was applied without source orientation constraints. Please note that without using the orientation constraint only the temporal dynamics of source powers can be obtained because each directional component of a cortical source vector has independent temporal dynamics. To apply the source orientation constraints, we need accurate individual anatomical data including structural MRI data, which unfortunately were not available in our experiments. Therefore, it will be necessary to develop new indices that can better measure the cortico-cortical functional connectivity, when the cortical orientation constraints are not imposed. Since the use of high-quality individual MRI data would make it possible to apply various functional connectivity measures such as phase coherence and phase locking value as well as would enhance the reliability of the source imaging results, we will try to use individual MRI data for real-time cortical connectivity imaging in our future studies. In addition, proper identification of ROIs on the cortical surface should be studied as a general issue in the source-level connectivity analyses [49]. In the present study, we also determined the locations and sizes of ROIs without applying a well-established criterion, which should be studied further. In the present study, we performed the cortical source imaging with only 32-channel EEG signals because we did not have a higher density EEG recording system. Since the use of more EEG electrodes would enhance the source imaging accuracy, we will apply the implemented software to other EEG systems with more recording channels.

Functional connectivity patterns associated with various cognitive or sensory tasks have been extensively investigated to characterize various psychiatric diseases such as schizophrenia [51, 53], Alzheimer's disease [52], and alexithymia [37]. Most offline analysis results have shown increased or decreased functional connectivity for specific frequency bands, thereby demonstrating the possibility of using connectivity information for noninvasive diagnoses of psychiatric diseases. We believe that our system also has the potential to be applied to the diagnosis of psychiatric diseases and further clinical investigations will be conducted in our future studies in cooperation with psychiatrists. Moreover, since it is known that functional connectivity is modulated at different sleep stages [36], it may be possible to use our system as a supplementary tool to monitor subjects' sleep stages in sleep studies or to watch if subjects fall asleep while performing a cognitive task. Another potential application that we are considering is an EEG-based brain–computer interface (BCI). Many recent studies on BCI have reported that the complementary use of conventional power density-based features and functional connectivity-based features could enhance the overall classification accuracies of BCI systems [3, 14, 56]. Since cortical source imaging is becoming a promising tool for the enhancement of the performance of EEG-based BCI systems [24, 25], a promising topic will be to combine the real-time dynamic neuroimaging system with the real-time cortical functional connectivity imaging system for extracting new BCI features.

In the present study, we implemented an EEG-based real-time cortical functional connectivity imaging system, but the same concept can also be applied to MEG without major modifications. In MEG, source-level analysis is relatively more important than in EEG because the MEG sensors are not attached directly on the subject's scalp surface. For example, if a subject's head is tilted in a helmet-type MEG system, so that one hemisphere is closer to the sensors than the other is, one could observe stronger activity at sensors closer to the subject's head even when the strengths are equal at the cortical level. Therefore, the real-time cortical functional connectivity imaging system can also be a useful tool in MEG studies. We are currently

developing new paradigms to diagnose various psychiatric diseases and also trying to generalize the operating software so as to release it worldwide to potential users.

Acknowledgments This work was supported in part by the KRISS-WCL project (Development of Measurement Technology for Cognitive Process) and in part by the Original Technology Research Program for Brain Science through the National Research Foundation of Korea (NRF) grant funded by the Ministry of Education, Science and Technology (No. 2010-0018840)

References

1. Astolfi L, Cincotti F, Mattia D, Fallani FDV, Tocci A, Colosimo A, Salinari S, Marciani MG, Hesse W, Witte H, Ursino M, Zavaglia M, Babiloni F (2008) Tracking the time-varying cortical connectivity patterns by adaptive multivariate estimators. IEEE Trans Biomed Eng 55(3):902–913
2. Bentin S, Allison T, Puce A, Perez E, McCarthy G (1996) Electrophysiological studies of face perception in humans. J Cogn Neurosci 8:551–565
3. Brunner C, Scherer R, Graimann B, Supp G, Pfurtscheller G (2006) Online control of a brain-computer interface using phase synchronization. IEEE Trans Biomed Eng 53(12):2501–2506
4. Coben R (2008) Assessment guided neurofeedback for ASD: EEG analyses. Appl Psychophys Biof 33:176
5. Coben R (2010) Efficacy of connectivity guided neurofeedback on language functions and IQ in autistic children. Appl Psychophys Biof 35:179
6. Coben R, Myers TE (2010) The relative efficacy of connectivity guided and symptom based EEG biofeedback for autistic disorders. Appl Psychophys Biof 35:13–23
7. David O, Cosmelli D, Friston KJ (2004) Evaluation of different measures of functional connectivity using a neural mass model. Neuroimage 21(2):659–673
8. Delorme A, Makeig S (2004) EEGLAB: an open source toolbox for analysis of single-trial EEG dynamics including independent component analysis. J Neurosci Methods 134(1):9–21
9. Evans AC, Collins DL, Milner B (1992) An MRI-based stereotactic atlas from 250 young normal subjects. J Soc Neurosci Abstr (18):408
10. Fingelkurts AA, Kallio S, Revonsuo A (2007) Cortex functional connectivity as a neurophysiological correlate of hypnosis: an EEG case study. Neuropsychologia 45(7):1452–1462
11. Fischl B, Sereno MI, Dale AM (1999) Cortical surface-based analysis. II: Inflation, flattening, and a surface-based coordinate system. Neuroimage 9(2):195–207
12. Fonteneau E, Davidoff J (2007) Neural correlates of colour categories. Neuroreport 18:1323–1327
13. Gow DW Jr, Segawa JA, Ahlfors SP, Lin FH (2008) Lexical influences on speech perception: a Granger causality analysis of MEG and EEG source estimates. Neuroimage 43(3):614–623
14. Gysels E, Celka P (2004) Phase synchronization for the recognition of mental tasks in a brain-computer interface. IEEE Trans Neural Syst Rehabil Eng 12(4):406–415
15. Hampson M, Peterson BS, Skudlarski P, Gatenby JC, Gore JC (2002) Detection of functional connectivity using temporal correlations in MR images. Hum Brain Mapp 15(4):247–262
16. Haueisen J, Ramon C, Eiselt M, Brauer H, Nowak H (1997) Influence of tissue resistivities on neuromagnetic fields and electric potentials studied with a finite element model of the head. IEEE Trans Biomed Eng 44(8):727–735
17. Hillyard SA, Anllo-Vento L (1998) Event-related brain potentials in the study of visual selective attention. Proc Natl Acad Sci USA 95:781–787
18. Hoechstetter K, Bornfleth H, Weckesser D, Ille N, Berg P, Scherg M (2004) BESA source coherence: a new method to study cortical oscillatory coupling. Brain Topogr 16(4):233–238
19. Holmes A, Franklin A, Clifford A, Davies I (2009) Neurophysiological evidence for categorical perception of color. Brain Cogn 69:426–434
20. Hwang HJ, Kwon K, Im CH (2009) Neurofeedback-based motor imagery training for brain-computer interface (BCI). J Neurosci Methods 179(1):150–156
21. Ibric VL, Dragomirescu LG, Hudspeth WJ (2009) Real-time changes in connectivities during neurofeedback. J Neurother 13:156–165
22. Im CH, Hwang HJ, Che H, Lee S (2007) An EEG-based real-time cortical rhythmic activity monitoring system. Physiol Meas 28(9):1101–1113
23. Im CH, Jung YJ, Lee S, Koh D, Kim DW, Kim BM (2010) Estimation of directional coupling between cortical areas using near-infrared spectroscopy (NIRS). Opt Exp 18(6):5730–5739
24. Kamousi B, Liu ZM, He B (2005) Classification of motor imagery tasks for brain-computer interface applications by means of two equivalent dipoles analysis. IEEE Trans Neural Syst Rehabil Eng 13(2):166–171
25. Kamousi B, Amini AN, He B (2007) Classification of motor imagery by means of cortical current density estimation and Von Neumann entropy. J Neural Eng 4(2):17–25
26. Keren AS, Yuval-Greenberg S, Deouell LY (2010) Saccadic spike potentials in gamma-band EEG: characterization, detection and suppression. Neuroimage 49:2248–2263
27. Kim KH, Choi JW, Yoon J (2009) Difference in gamma-band phase synchronization during semantic processing of visually presented words from primary and secondary languages. Brain Res 1291:82–91
28. Koenig T, Lehmann D, Saito N, Kuginuki T, Kinoshita T, Koukkou M (2001) Decreased functional connectivity of EEG theta-frequency activity in first-episode, neuroleptic-naive patients with schizophrenia: preliminary results. Schizophr Res 50(1–2):55–60
29. Korzeniewska A, Crainiceanu CM, Kus R, Franaszczuk PJ, Crone NE (2008) Dynamics of event-related causality in brain electrical activity. Hum Brain Mapp 29(10):1170–1192
30. Le Van Quyen M, Bragin A (2007) Analysis of dynamic brain oscillations: methodological advances. Trends Neurosci 30(7):365–373
31. Lee SH, Kim DW, Kim EY, Kim S, Im CH (2010) Dysfunctional gamma-band activity during face structural processing in schizophrenia patients. Schizophr Res 119:191–197
32. Leuchter AF, Newton TF, Cook IA, Walter DO, Rosenberg-Thompson S, Lachenbruch PA (1992) Changes in brain functional connectivity in Alzheimer-type and multi-infarct dementia. Brain 115(Pt 5):1543–1561
33. Lin FH, Witzel T, Hamalainen MS, Dale AM, Belliveau JW, Stufflebeam SM (2004) Spectral spatiotemporal imaging of cortical oscillations and interactions in the human brain. Neuroimage 23(2):582–595
34. Liu AK, Dale AM, Belliveau JW (2002) Monte Carlo simulation studies of EEG and MEG localization accuracy. Hum Brain Mapp 16:47–62
35. Manganotti P, Gerloff C, Toro C, Katsuta H, Sadato N, Zhuang P, Leocani L, Hallett M (1998) Task-related coherence and task-related spectral power changes during sequential finger movements. Electroencephalogr Clin Neurophysiol 109:50–62
36. Massimini M, Ferrarelli F, Huber R, Esser SK, Singh H, Tononi G (2005) Breakdown of cortical effective connectivity during sleep. Science 309(5744):2228–2232

37. Matsumoto A, Ichikawa Y, Kanayama N, Ohira H, Iidaka T (2006) Gamma band activity and its synchronization reflect the dysfunctional emotional processing in alexithymic persons. Psychophysiology 43(6):533–540
38. McMenamin BW, Shackman AJ, Maxwell JS, Bachhuber DRW, Koppenhaver AM, Greischar LL, Davidson RJ (2010) Validation of ICA-based myogenic artifact correction for scalp and source-localized EEG. Neuroimage 49:2416–2432
39. Menon V, Freeman WJ, Cutillo BA, Desmond JE, Ward MF, Bressler SL, Laxer KD, Barbaro N, Gevins AS (1996) Spatio-temporal correlations in human gamma band electrocorticograms. Electroencephalogr Clin Neurophysiol 98(2):89–102
40. Mormann F, Lehnertz K, David P, Elger CE (2000) Mean phase coherence as a measure for phase synchronization and its application to the EEG of epilepsy patients. Phys D 144(3–4):358–369
41. Murias M, Webb SJ, Greenson J, Dawson G (2007) Resting state cortical connectivity reflected in EEG coherence in individuals with autism. Biol Psychiatry 62(3):270–273
42. Oostendorp TF, Delbeke J, Stegeman DF (2000) The conductivity of the human skull: results of in vivo and in vitro measurements. IEEE Trans Biomed Eng 47(11):1487–1492
43. Park YM, Che HJ, Im CH, Jung HT, Bae SM, Lee SH (2008) Decreased EEG synchronization and its correlation with symptom severity in Alzheimer's disease. Neurosci Res 62(2):112–117
44. Peled A, Geva AB, Kremen WS, Blankfeld HM, Esfandiarfard R, Nordahl TE (2001) Functional connectivity and working memory in schizophrenia: an EEG study. Int J Neurosci 106(1–2):47–61
45. Pfurtscheller G, Andrew C (1999) Event-related changes of band power and coherence: methodology and interpretation. J Clin Neurophysiol 16(6):512–519
46. Reijneveld JC, Ponten SC, Berendse HW, Stam CJ (2007) The application of graph theoretical analysis to complex networks in the brain. Clin Neurophysiol 118(11):2317–2331
47. Rubinov M, Sporns O (2010) Complex network measures of brain connectivity: uses and interpretations. Neuroimage 52: 1059–1069
48. Sarnthein J, Petsche H, Rappelsberger P, Shaw GL, von Stein A (1998) Synchronization between prefrontal and posterior association cortex during human working memory. Proc Natl Acad Sci USA 95:7092–7096
49. Schoffelen JM, Gross J (2009) Source connectivity analysis with MEG and EEG. Hum Brain Mapp 30(6):1857–1865
50. Shattuck DW, Leahy RM (2002) BrainSuite: an automated cortical surface identification tool. Med Image Anal 6(2):129–142
51. Spencer KM, Nestor PG, Niznikiewicz MA, Salisbury DF, Shenton ME, McCarley RW (2003) Abnormal neural synchrony in schizophrenia. J Neurosci 23(19):7407–7411
52. Stam CJ, Jones BF, Nolte G, Breakspear M, Scheltens P (2007) Small-world networks and functional connectivity in Alzheimer's disease. Cereb Cortex 17(1):92–99
53. Uhlhaas PJ, Linden DEJ, Singer W, Haenschel C, Lindner M, Maurer K, Rodriguez E (2006) Dysfunctional long-range coordination of neural activity during Gestalt perception in schizophrenia. J Neurosci 26(31):8168–8175
54. Verdoux H, Cougnard A, Grolleau S, Besson R, Delcroix F (2005) How do general practitioners manage subjects with early schizophrenia and collaborate with mental health professionals? A postal survey in South-Western France. Soc Psychiatry Psychiatr Epidemiol 40(11):892–898
55. Vuilleumier P, Pourtois G (2007) Distributed and interactive brain mechanisms during emotion face perception: evidence from functional neuroimaging. Neuropsychologia 45:174–194
56. Wei QG, Wang YJ, Gao XR, Gao SK (2007) Amplitude and phase coupling measures for feature extraction in an EEG-based brain-computer interface. J Neural Eng 4(2):120–129